Accurate Biot-Savart Routines with Correct Asymptotic Behavior

Jonathan Schilling[a,*], Jakob Svensson[a], Udo Höfel[a], Joachim Geiger[a]

[a]*Max-Planck-Institute for Plasma Physics, Wendelsteinstrasse 1, 17489 Greifswald, Germany*

Abstract

A set of routines to compute the magnetic vector potential and magnetic field of two types of current carriers is presented. The (infinitely thin) current carrier types are a straight wire segment and a circular wire loop. The routines are highly accurate and exhibit the correct asymptotic behavior far away from and close to the current carrier. A suitable global set of test points is introduced and the methods presented in this work are tested against results obtained using arbitrary-precision arithmetic on all test points. The results are accurate to approximately 16 decimal digits of precision when computed using 64 bit floating point arithmetic, with few exceptions where accuracy drops to 13 digits. These primitive types can be used to make up more complex current carrier arrangements, such as a current along a polygon (by means of defining straight wire segments from point to point of the polygon) and a multi-winding coil with circular cross-section (by positioning circular wire loops at appropriate positions in the coils cross-section). Reference data is provided along with the code to compute it for testing the reader's routines against this work.

Keywords: magnetostatics; Biot-Savart; straight wire segment; circular wire loop; magnetic vector potential; magnetic field

PROGRAM SUMMARY

Program Title: Accurate Biot-Savart routines with Correct Asymptotic Behavior
CPC Library link to program files: (to be added by Technical Editor)

---

[*]Corresponding author.
E-mail address: jonathan.schilling@ipp.mpg.de

Developer's repository link: https://github.com/jonathanschilling/abscab

Code Ocean capsule: (to be added by Technical Editor)

Licensing provisions(please choose one): Apache-2.0

Programming language: C, Python, Java, Fortran

Supplementary material: Reference output data for all methods described in this article.

Nature of problem(approx. 50-250 words):

Solution method(approx. 50-250 words):

Additional comments including restrictions and unusual features (approx. 50-250 words):

The implementations provided here have not been optimized for speed.

References

[1] Reference 1

[2] Reference 2

[3] Reference 3

1. Introduction

Usually, the magnetic field is denoted by $\mathbf{H}$ and the magnetic flux density $\mathbf{B}$ is then given by $\mathbf{B} = \mu_0 \mu_{\mathrm{r}} \mathbf{H}$, where μ_0 is the vacuum magnetic permeability and μ_r is the relative permeability, taking material properties into account. In the field of plasma physics generally and in this work in particular, these two terms are frequently used synonymously due to the vanishing magnetic susceptibility $|\chi| \ll 1$ of the plasma, leading to $\mu_r = 1 + \chi \approx 1$. Then, magnetic field and magnetic flux density only differ by a factor of μ_0.

2. Methods

In this section, accurate methods used to compute the magnetic vector potential and the magnetic field of a straight wire segment and a circular wire loop are presented. Furthermore, methods to evaluate the magnetostatic quantities in Cartesian coordinates are provided. The section is concluded by a description of the verification procedure employed to benchmark these methods.

2.1. Straight Wire Segment

The straight wire segment is handled first. The basic geometry of a single wire segment is shown in Fig. 1.
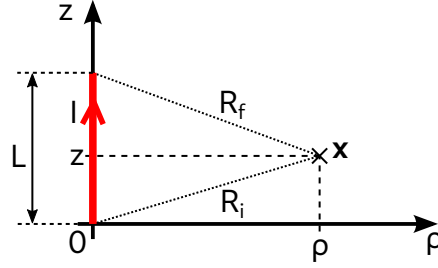

Figure 1: Geometry of a single wire segment. After Fig. 1 in Ref. [1].

2.1.1. Magnetic Vector Potential

The magnetic vector potential of a straight wire segment only has component A_z parallel to the wire:

$$\mathbf{A} = A_z \hat{\mathbf{e}}_z .$$ (1)

It is given by:

$$A_z(\rho, z) = \frac{\mu_0 I}{4\pi} \ln \left(\frac{1 + \epsilon}{1 - \epsilon} \right)$$ (2)

with

$$\epsilon = \frac{L}{R_i + R_f}$$ (3)

$$R_i = \sqrt{\rho^2 + z^2}$$ (4)

$$R_f = \sqrt{\rho^2 + (1 - z)^2} .$$ (5)

4

Here, we use normalized coordinates $\rho' = \rho/L$ and $z' = z/L$. This leads to the following expressions for $r_{\mathrm{i}} = R_{\mathrm{i}}/L$ and $r_{\mathrm{f}} = R_{\mathrm{f}}/L$:

$$r_{\mathrm{i}} = \sqrt{\rho'^2 + z'^2} \tag{6}$$

$$r_{\mathrm{f}} = \sqrt{\rho'^2 + (1 - z')^2} \tag{7}$$

$$\epsilon = \frac{1}{r_{\mathrm{i}} + r_{\mathrm{f}}} \, . \tag{8}$$

A common prefactor depending on the current I and μ_0 is split off:

$$A_z(\rho, z) = \frac{\mu_0 I}{2\pi} \tilde{A}_z(\rho', z') \tag{9}$$

with

$$\tilde{A}_z(\rho', z') = \frac{1}{2} \ln\left(\frac{1 + \epsilon}{1 - \epsilon}\right) = \operatorname{atanh}(\epsilon) \, . \tag{10}$$

The rest of this section is dedicated to the accurate computation of $\tilde{A}_z(\rho', z')$. One of several formulations is chosen depending on the evaluation location (ρ', z'):

$$\tilde{A}_z(\rho', z') = \begin{cases} \tilde{A}_{\mathrm{z,ax}}(z') & : \rho' = 0, \text{ any } z' \\ \tilde{A}_{\mathrm{z,rad}}(\rho') & : \text{any } \rho', z' \in \{0, 1\} \\ \tilde{A}_{\mathrm{z,f}}(\rho', z') & : \rho' \geq 1 \text{ or } z' \leq 1 \text{ or } z' > 2 \\ \tilde{A}_{\mathrm{z,n}}(\rho', z') & : \text{else} \, . \end{cases} \tag{11}$$

For the case $\rho' = 0$, the following formulation is used:

$$\tilde{A}_{\mathrm{z,ax}}(z') = \begin{cases} \tilde{A}_{\mathrm{z,ax,f}}(z') & : z' < -1 \text{ or } z' > 2 \\ \tilde{A}_{\mathrm{z,ax,n}}(z') & : \text{else} \end{cases} \tag{12}$$

with

$$\tilde{A}_{\mathrm{z,ax,f}}(z') = \operatorname{atanh}\left(\frac{1}{|z'| + |1 - z'|}\right) \tag{13}$$

and

$$\tilde{A}_{\mathrm{z,ax,n}}(z') = \frac{1}{2} \frac{z'}{|z'|} \ln\left(\left|\frac{z'}{1 - z'}\right|\right) \, . \tag{14}$$

5

The following formulation is used for the cases $z' = 0$ or $z' = 1$:

$$\tilde{A}_{\text{z,rad}}(\rho') = \begin{cases} \tilde{A}_{\text{z,rad,f}}(\rho') & : \rho' > 1 \\ \tilde{A}_{\text{z,rad,n}}(\rho') & : \text{else} \end{cases} \tag{15}$$

with

$$\tilde{A}_{\text{z,rad,f}}(z') = \operatorname{atanh}\left(\frac{1}{\rho' + \sqrt{\rho'^2 + 1}}\right) \tag{16}$$

and

$$\tilde{A}_{\text{z,rad,n}}(z') = \frac{1}{2}\ln\left(\frac{\rho'c + 1 + c}{\rho'c + 2s^2}\right), \tag{17}$$

where

$$c = \frac{1}{\sqrt{\rho'^2 + 1}} \tag{18}$$

$$s = \sin(\arctan(\rho')/2). \tag{19}$$

The case of $\tilde{A}_{\text{z,f}}(\rho', z')$ is implemented as:

$$\tilde{A}_{\text{z,f}}(\rho', z') = \operatorname{atanh}(\epsilon) \tag{20}$$

with r_i, r_f and ϵ from Eqn. (6), Eqn. (7) and Eqn. (8), respectively. The final case is implemented as follows:

$$\tilde{A}_{\text{z,n}}(\rho', z') = \frac{1}{2}\left[\ln(n + 2) - \ln(n)\right] \tag{21}$$

with

$$n = (r_\text{i} - z') + (r_\text{f} - (1 - z')) \tag{22}$$
$$r_\text{i} - z' = 2r_\text{i}\sin^2(\alpha/2) \tag{23}$$
$$r_\text{f} - (1 - z') = 2r_\text{f}\sin^2(\beta/2) \tag{24}$$
$$\alpha = \texttt{atan2}(\rho', z') \tag{25}$$
$$\beta = \texttt{atan2}(\rho', 1 - z'). \tag{26}$$

2.1.2. Magnetic Field

The magnetic field of a straight wire segment is given by [1]:

$$\mathbf{B} = \frac{\mu_0 I}{4\pi} \hat{\mathbf{e}}_z \times \mathbf{R}_i \frac{2L(R_i + R_f)}{R_i R_f} \frac{1}{(R_i + R_f)^2 - L^2} .\tag{27}$$

The vector $\mathbf{R}_i$ has components in directions parallel (z) and perpendicular (ρ) to the wire segment:

$$\mathbf{R}_i = z\,\hat{\mathbf{e}}_z + \rho\,\hat{\mathbf{e}}_\rho \tag{28}$$

where ρ and z are cylindrical coordinates in the coordinate system aligned with the wire segment. The vector-valued term in Eqn. (27) is reformulated as follows:

$$\begin{aligned}
\hat{\mathbf{e}}_z \times \mathbf{R}_i &= \hat{\mathbf{e}}_z \times (z\,\hat{\mathbf{e}}_z + \rho\,\hat{\mathbf{e}}_\rho) \\
&= z\underbrace{\hat{\mathbf{e}}_z \times \hat{\mathbf{e}}_z}_{=0} + \rho\underbrace{\hat{\mathbf{e}}_z \times \hat{\mathbf{e}}_\rho}_{=\hat{\mathbf{e}}_\varphi} = \rho\,\hat{\mathbf{e}}_\varphi .
\end{aligned}\tag{29}$$

It follows that the magnetic field of a straight wire segment only has a component B_φ in tangential direction:

$$\mathbf{B} = B_\varphi \hat{\mathbf{e}}_\varphi \tag{30}$$

with

$$B_\varphi(\rho, z) = \frac{\mu_0 I}{4\pi} \frac{2\rho L(R_i + R_f)}{R_i R_f} \frac{1}{(R_i + R_f)^2 - L^2} .\tag{31}$$

This is now reformulated to use normalized quantities (as done above for the computation of the magnetic vector potential):

$$B_\varphi = \frac{\mu_0 I}{4\pi L} \left(\frac{1}{r_f} + \frac{1}{r_i}\right) \frac{2\rho'}{(r_i + r_f)^2 - 1} .\tag{32}$$

Again a normalization factor is split off:

$$B_\varphi(\rho, z) = \frac{\mu_0 I}{4\pi L} \tilde{B}_\varphi(\rho', z') \tag{33}$$

with

$$\tilde{B}_\varphi(\rho', z') = \left(\frac{1}{r_f} + \frac{1}{r_i}\right) \frac{2\rho'}{(r_i + r_f)^2 - 1} .\tag{34}$$

7

Consider the denominator in more detail:

$$
\begin{aligned}
(r_\mathrm{i} + r_\mathrm{f})^2 - 1 &= r_\mathrm{i}^2 + 2r_\mathrm{i}r_\mathrm{f} + r_\mathrm{f}^2 - 1 \\
&= \rho'^2 + z'^2 + 2r_\mathrm{i}r_\mathrm{f} + \rho'^2 + (1 - z')^2 - 1 \\
&= \rho'^2 + z'^2 + 2r_\mathrm{i}r_\mathrm{f} + \rho'^2 + \cancel{1} - 2z' + z'^2 \cancel{-1} \\
&= 2\rho'^2 + 2z'^2 + 2r_\mathrm{i}r_\mathrm{f} - 2z' \\
&= 2\left[\rho'^2 + r_\mathrm{i}r_\mathrm{f} - z'(1 - z')\right] .
\end{aligned}
\tag{35}
$$

This leads to:

$$
\tilde{B}_\varphi(\rho', z') = \left(\frac{1}{r_\mathrm{f}} + \frac{1}{r_\mathrm{i}}\right) \frac{\cancel{2}\rho'}{\cancel{2}\left[\rho'^2 + r_\mathrm{i}r_\mathrm{f} - z'(1 - z')\right]} .
\tag{36}
$$

One of several formulations is chosen depending on the evaluation location (ρ', z'):

$$
\tilde{B}_\varphi(\rho', z') =
\begin{cases}
0 & : \rho' = 0, \text{ any } z' \\
\tilde{B}_{\varphi,\mathrm{rad}}(\rho') & : \text{any } \rho', z' \in \{0, 1\} \\
\tilde{B}_{\varphi,\mathrm{f}}(\rho', z') & : \rho' \geq 1 \text{ or } z' \leq 0 \text{ or } z' \geq 1 \\
& \quad \text{or } \rho'/(1 - z') \geq 1 \\
& \quad \text{or } \rho'/z' \geq 1 \\
\tilde{B}_{\varphi,\mathrm{n}}(\rho', z') & : \text{else} .
\end{cases}
\tag{37}
$$

The special case $z' \in \{0, 1\}$ is implemented as follows:

$$
\tilde{B}_{\varphi,\mathrm{rad}}(\rho') = \frac{1}{\rho'\sqrt{\rho'^2 + 1}} .
\tag{38}
$$

The formula in Eqn. (36) is used for evaluation locations far away from the wire as well as a part of the near-field close to the wire segment:

$$
\tilde{B}_{\varphi,\mathrm{f}}(\rho', z') = \left(\frac{1}{r_\mathrm{f}} + \frac{1}{r_\mathrm{i}}\right) \frac{\rho'}{\rho'^2 + r_\mathrm{i}r_\mathrm{f} - z'(1 - z')} .
\tag{39}
$$

The final case is implemented as follows:

$$
\tilde{B}_{\varphi,\mathrm{n}}(\rho', z') = \left(\frac{1}{r_\mathrm{f}} + \frac{1}{r_\mathrm{i}}\right) \frac{\rho'}{\rho'^2 + 2r_\mathrm{i}\left[r_\mathrm{f}\sin^2(\beta/2) + (1 - z')\sin^2(\alpha/2)\right]}
\tag{40}
$$

with α and β from Eqn. (25) and Eqn. (26), respectively.

2.2. Circular Wire Loop

The circular wire loop is handled next. The basic geometry of a circular wire loop under consideration here is shown in Fig. 2.

Figure 2: Geometry of a circular wire loop centered at the origin with normal vector aligned with the z-axis. The radius of the loop is denoted a and a current I flows in the indicated direction. The magnetic field and vector potential are to be evaluated at the point $\mathbf{x}$ in the (x, z)-plane.

Similar to the case of the straight wire segment, the magnetic vector potential and the magnetic field of the circular wire loop are assembled from various formulations for special cases of the far-field and the near-field.

2.2.1. Magnetic Vector Potential

The magnetic vector potential of a circular wire loop only has a tangential component A_φ. In Eqn. (5.37) of Ref. [2], A_φ is expressed as follows for a loop of radius a and current I along it:

$$A_\varphi(r, \theta) = \frac{\mu_0}{4\pi} \frac{4Ia}{\sqrt{a^2 + r^2 + 2ar\sin(\theta)}} \left[\frac{(2 - k^2)\mathcal{K}(k) - 2\mathcal{E}(k)}{k^2} \right] \tag{41}$$

with

$$k^2 = \frac{4ar\sin(\theta)}{a^2 + r^2 + 2ar\sin(\theta)} . \tag{42}$$

Here, $\mathcal{K}(k)$ and $\mathcal{E}(k)$ are the complete elliptic integrals of the first and second kind, respectively. Spherical coordinates (r, θ) are used to specify the evaluation location. The corresponding normalized cylindrical coordinates (ρ', z') are given by $\rho' = r\sin(\theta)/a$ and $z' = \sqrt{r^2 - \rho^2}/a$. An expression for the

9

linear combination of $\mathcal{K}(k)$ and $\mathcal{E}(k)$ from Ref. [3] is used to reformulate the expression provided by Jackson:

$$\lambda \mathcal{K}(k) + \mu \mathcal{E}(k) = \operatorname{cel}(k_c, 1, \lambda + \mu, \lambda + \mu k_c^2) \tag{43}$$

where

$$k_c^2 = 1 - k^2 . \tag{44}$$

The argument of the elliptic integrals is considered first:

$$
\begin{aligned}
k^2 &= \frac{4ar\sin(\theta)}{a^2 + r^2 + 2ar\sin(\theta)} = \frac{4a\rho}{a^2 + r^2 + 2a\rho} = \frac{4a\rho}{a^2\left(1 + \frac{r^2}{a^2} + 2\frac{\rho}{a}\right)} \\
&= \frac{4\rho'}{1 + \frac{r^2}{a^2} + 2\rho'} = 4\rho'\left(1 + \frac{\rho^2 + z^2}{a^2} + 2\rho'\right)^{-1} \\
&= 4\rho'\left(1 + \rho'^2 + z'^2 + 2\rho'\right)^{-1} = \frac{4\rho'}{z'^2 + (1 + \rho')^2} .
\end{aligned}
\tag{45}
$$

This implies:

$$k_c^2 = \frac{z'^2 + (1 - \rho')^2}{z'^2 + (1 + \rho')^2} . \tag{46}$$

The coefficients of the elliptic integrals are identified as follows:

$$\lambda = \frac{2 - k^2}{k^2} = \frac{2}{k^2} - 1 \tag{47}$$

$$\mu = -\frac{2}{k^2} \tag{48}$$

and their combinations are as follows:

$$\lambda + \mu = \frac{2}{k^2} - 1 - \frac{2}{k^2} = -1 \tag{49}$$

$$
\begin{aligned}
\lambda + \mu k_c^2 &= \frac{2}{k^2} - 1 - \frac{2}{k^2}(1 - k^2) \\
&= \frac{2}{k^2} - 1 - \frac{2}{k^2} + 2 = 1 .
\end{aligned}
\tag{50}
$$

Putting above results together, we arrive at the following expression for A_φ:

$$A_\varphi(\rho', z') = \frac{\mu_0 I}{\pi} \frac{1}{\sqrt{z'^2 + (1 + \rho')^2}} \operatorname{cel}(k_c, 1, -1, 1) . \tag{51}$$

10

It is favorable for numerical evaluation of A_φ to use the form given in Eqn. (51) where the linear combination of the complete elliptic integrals is embedded in the parameters of $\text{cel}(k_c, p, a, b)$ and less precautions need to be taken to deal with cancellations in Eqn. (41). A physics-oriented prefactor is split off to be able to focus on geometry in the following:

$$A_\varphi(\rho', z') = \frac{\mu_0 I}{\pi} \tilde{A}_\varphi(\rho', z') \tag{52}$$

with

$$\tilde{A}_\varphi(\rho', z') = \frac{1}{\sqrt{z'^2 + (1 + \rho')^2}} \, \text{cel}(k_c, 1, -1, 1) \,. \tag{53}$$

One of several formulations is chosen depending on the evaluation location (ρ', z'):

$$\tilde{A}_\varphi(\rho', z') = \begin{cases} 0 & : \rho' = 0, \text{ any } z' \\ \tilde{A}_{\varphi,\text{f}}(\rho', z') & : \rho' < 1/2 \text{ or } \rho' > 2 \text{ or } |z'| \geq 1 \\ \tilde{A}_{\varphi,\text{n}}(\rho', z') & : 1/2 \leq \rho' \leq 2 \text{ but } \rho' \neq 1, |z'| < 1 \\ \tilde{A}_{\varphi,\text{v}}(\rho', z') & : \text{else} \,. \end{cases} \tag{54}$$

The following formula is implemented for evaluation locations away from the wire loop:

$$\tilde{A}_{\varphi,\text{f}}(\rho', z') = \frac{k^2}{\sqrt{z'^2 + (1 + \rho')^2}} \, \mathcal{C}(k_c) \tag{55}$$

with k^2 from Eqn. (45) and

$$\mathcal{C}(k_c) = \text{cel}\left(\frac{2\sqrt{k_c}}{1 + k_c}, 1, 0, \frac{2}{(1 + k_c)^3}\right) \,. \tag{56}$$

Close to the wire loop, the following formulation is used:

$$\tilde{A}_{\varphi,\text{n}}(\rho', z') = \frac{1}{|\rho' - 1|\sqrt{\left(\frac{z'}{\rho'-1}\right)^2 + \left(1 + \frac{2}{\rho'-1}\right)^2}} \, \text{cel}(\sqrt{k_c^2}, 1, -1, 1) \tag{57}$$

with k_c^2 computed as follows:

$$k_c^2 = \frac{\left(\frac{z'}{\rho'-1}\right)^2 + 1}{\left(\frac{z'}{\rho'-1}\right)^2 + \left(1 + \frac{2}{\rho'-1}\right)^2} \,. \tag{58}$$

11

At $\rho' = 1$, some further simplification can be carried out. This leads to the following formulation for $\rho' = 1$ and $|z'| < 1$:

$$\tilde{A}_{\varphi,\text{v}}(\rho' = 1, z') = \frac{1}{|z'|} \operatorname{cel}(k_c, 1, 1, -1) \tag{59}$$

with k_c computed as follows:

$$k_c = \frac{1}{|z'|} \sqrt{4 + z'^2}\,. \tag{60}$$

2.2.2. Magnetic Field

The magnetic field produced by a circular wire loop is made up of two components: B_ρ denotes the radial component and B_z denotes the vertical component. The radial component B_ρ is given by:

$$B_\rho(\rho', z') = \frac{\mu_0 I}{\pi a} \frac{z'}{[z'^2 + (1 + \rho')^2]^{\frac{3}{2}}} \operatorname{cel}(k_c, k_c^2, -1, 1) \tag{61}$$

Also here, a normalization factor is split off:

$$B_\rho(\rho, z) = \frac{\mu_0 I}{\pi a} \tilde{B}_\rho(\rho', z') \tag{62}$$

with

$$\tilde{B}_\rho(\rho', z') = \frac{z'}{[z'^2 + (1 + \rho')^2]^{\frac{3}{2}}} \operatorname{cel}(k_c, k_c^2, -1, 1)\,. \tag{63}$$

One of several formulations is chosen depending on the evaluation location (ρ', z'):

$$\tilde{B}_\rho(\rho', z') = \begin{cases} 0 & : \rho' = 0, \text{ any } z' \\ & \quad \text{or any } \rho', z' = 0 \\ \tilde{B}_{\rho,\text{f}}(\rho', z') & : \rho' < 1/2 \text{ or } \rho' > 2 \text{ or } |z'| \geq 1 \\ \tilde{B}_{\rho,\text{n}}(\rho', z') & : 1/2 \leq \rho' \leq 2 \text{ but } \rho' \neq 1, |z'| < 1 \\ \tilde{B}_{\rho,\text{v}}(z') & : \text{else}\,. \end{cases} \tag{64}$$

The following formulation is implemented for evaluation locations away from to the wire loop:

$$\tilde{B}_{\rho,\text{f}}(\rho', z') = \frac{4\rho' z' \left[\mathcal{D}(k_c) - \mathcal{C}(k_c) \right]}{\left[z'^2 + (1 + \rho')^2 \right]^{3/2} \left[z'^2 + (1 - \rho')^2 \right]} \tag{65}$$

12

with
$$\mathcal{D}(k_c) = \frac{\mathcal{K}(k_c) - \mathcal{E}(k_c)}{k^2} = \operatorname{cel}(k_c, 1, 0, 1). \tag{66}$$

For points close to the wire loop, but with $\rho' \neq 1$, the following formulation is used:

$$\tilde{B}_{\rho,\mathrm{n}}(\rho', z') = \frac{4\rho'\left[\mathcal{D}(k_c) - \mathcal{C}(k_c)\right]}{(\rho'-1)^4 \left|\frac{z'}{\rho'-1}\right|}$$
$$\left\{\left[\left(\frac{z'}{\rho'-1}\right)^2 + \left(1 + \frac{2}{\rho'-1}\right)^2\right]^{3/2}\left[\left(\frac{z'}{\rho'-1}\right)^2 + 1\right]\right\}^{-1} \tag{67}$$

Finally, for $\rho' = 1$ and $|z'| < 1$, the following formulation is used:

$$\tilde{B}_{\rho,\mathrm{v}}(z') = \frac{1}{2\sqrt{1+4/z'^2}}\left[\frac{\mathcal{E}(k_c)}{1+4/z'^2}\left(1 + \frac{1}{z'^2}\left(6 + \frac{8}{z'^2}\right)\right) - \mathcal{K}(k_c)\right] \tag{68}$$

with
$$k_c^2 = \frac{1}{1+4/z'^2}. \tag{69}$$

The vertical component B_z of the magnetic field of a circular wire loop is given by:

$$B_z(\rho', z') = \frac{\mu_0 I}{2\pi a}\frac{1}{\rho'\sqrt{z'^2 + (1+\rho')^2}}$$
$$\left[\operatorname{cel}(k_c, 1, -1, 1) + \frac{1 + k_c^2 - (1 - k_c^2)\rho'}{2}\operatorname{cel}(k_c, k_c^2, -1, 1)\right] \tag{70}$$

One of several formulations is selected depending on the evaluation location (ρ', z'):

$$\tilde{B}_z(\rho', z') = \begin{cases} \tilde{B}_{z,1}(\rho', z') & : \rho' < 1/2 \text{ or } (\rho' < 2 \text{ and } z' \geq 1) \\ \tilde{B}_{z,2}(\rho', z') & : \rho' \geq 2 \\ \tilde{B}_{z,4}(\rho', z') & : \rho' = 1 \\ \tilde{B}_{z,5}(\rho', z') & : z' \neq 0 \\ \tilde{B}_{z,6}(\rho', z') & : \text{else} \end{cases} \tag{71}$$

TODO: There is a factor of 2 too much in the denominator of B_z!

13

Finally, a normalization factor is split off here as well:

$$B_z(\rho, z) = \frac{\mu_0 I}{2\pi a} \tilde{B}_z(\rho', z') \tag{72}$$

with

$$\tilde{B}_z(\rho', z') = \frac{1}{\rho' \sqrt{z'^2 + (1 + \rho')^2}}$$
$$\left[\mathrm{cel}(k_c, 1, -1, 1) + \frac{1 + k_c^2 - (1 - k_c^2)\rho'}{2} \mathrm{cel}(k_c, k_c^2, -1, 1) \right]. \tag{73}$$

The evaluation of this formula is split up as well into separate special cases. For points not too close to the wire loop, the following formulation is used:

$$\tilde{B}_{z,1}(\rho', z') = \frac{1}{\sqrt{z'^2 + (1 + \rho')^2} \left[z'^2 + (1 - \rho')^2 \right]}$$
$$\left[\mathcal{E}(k_c) + \rho' \left(\mathcal{E}(k_c) - 2\mathcal{K}(k_c) + 2\mathcal{D}(k_c) \right) \right]. \tag{74}$$

A second method is needed for points with $\rho' > 2$:

$$\tilde{B}_{z,2}(\rho', z') = \frac{1}{\sqrt{r_0}\rho'^3} \left[\mathcal{E}(k_c) + \frac{4}{t} \left(\mathcal{C}(k_c) - \mathcal{D}(k_c) \right) \right] \tag{75}$$

with

$$r_0 = 1 + \frac{1}{\rho'} \left[-2 + \frac{1}{\rho'} \left(3z'^2 - 1 + \frac{1}{\rho'} \left\{ -4z'^2 + 4 \right. \right. \right.$$
$$+ \frac{1}{\rho'} \left[3 \left(z'^2 + 1 \right)^2 - 4 \left(z'^2 + 1 \right) \right.$$
$$\left. \left. \left. \left. + \frac{1}{\rho'} \left(-2 \left(z'^2 + 1 \right)^2 + \frac{1}{\rho'} \left(z'^2 + 1 \right)^3 \right) \right] \right\} \right) \right] \tag{76}$$

and

$$t = 1 + \frac{1}{\rho'} \left(2 + \frac{1}{\rho'} \left[z'^2 + 1 \right] \right). \tag{77}$$

The expression for $\tilde{B}_z$ becomes significantly simpler at $\rho' = 1$, which is considered next:

$$\tilde{B}_{z,4}(\rho' = 1, z') = \frac{1}{\left[z'^2 + 4 \right]^{3/2}} \mathrm{cel}(\sqrt{k_c^2}, k_c^2, 2, 0) \tag{78}$$

14

with

$$k_c^2 = \frac{z'^2}{z'^2 + 4}.$$

(79)

In the vicinity of the wire loop, but explicitly obeying $z' \neq 0$, the following method should be used to compute $\tilde{B}_z$:

$$\tilde{B}_{z,5}(\rho', z') = \frac{\left|\frac{z'}{\rho'-1}\right| \mathrm{cel}\left(\sqrt{k_c^2}, k_c^2, \frac{1+\rho'}{z'}, \frac{1-\rho'}{z'}\right)}{(\rho' - 1)^2 \left[\left(\frac{z'}{\rho'-1}\right)^2 + \left(1 + \frac{2}{\rho'-1}\right)^2\right]^{3/2}}.$$

(80)

Finally, only one more expression is needed to accurately compute $\tilde{B}_z$ at $z' = 0$ close to the loop. Here it is:

$$\tilde{B}_{z,6}(\rho', z' = 0) = \frac{1}{|1 + \rho'|^3} \mathrm{cel}(k_c, k_c^2, 1 + \rho', 1 - \rho')$$

(81)

with

$$k_c = \frac{1 - \rho'}{1 + \rho'}.$$

(82)

2.3. Transformation to Cartesian Coordinates

Evaluation of the magnetic vector potential A and magnetic field B produced by the current carriers considered in this work happens in cylindrical coordinates ρ and z. It is often more convenient to be able to work in Cartesian coordinates. The methods given in this section show how to transform the evaluation location into cylindrical coordinates in the frame of reference of the current carrier and subsequently transform back the magnetostatic quantities into the global Cartesian coordinate system.

2.3.1. Straight Wire Segment

Figure 3 illustrates the setup of a straight wire segment.

The length of the wire segment is denoted by L:

$$L = |\mathbf{x}_f - \mathbf{x}_i|.$$

(83)

The unit vector along the segment $\hat{\mathbf{e}}_z$ is then computed as:

$$\hat{\mathbf{e}}_z = \frac{\mathbf{x}_f - \mathbf{x}_i}{L}.$$

(84)

Figure 3: Mapping the components to Cartesian coordinates for an exemplary straight wire segment. The wire segment is positioned from $\mathbf{x}_i$ to $\mathbf{x}_f$. Its parallel unit vector is denoted $\hat{\mathbf{e}}_z$. The length of the wire segment is denoted by L. The evaluation location is denoted by $\mathbf{r}$.

The vertical coordinate z in the coordinate system of the wire segment is:

$$z = (\mathbf{r} - \mathbf{x}_i) \cdot \hat{\mathbf{e}}_z \tag{85}$$

and the normalized z-coordinate is:

$$z' = \frac{z}{L} = \frac{1}{L}(\mathbf{r} - \mathbf{x}_i) \cdot \hat{\mathbf{e}}_z \,. \tag{86}$$

For the radial coordinate, first the vector $\Delta\mathbf{r}$ is formed:

$$\Delta\mathbf{r} = (\mathbf{r} - \mathbf{x}_i) - z\,\hat{\mathbf{e}}_z \tag{87}$$

and the radial coordinate ρ is then obtained by taking $\rho = |\Delta\mathbf{r}|$. A unit vector in radial direction is formed as follows:

$$\hat{\mathbf{e}}_\rho = \frac{\Delta\mathbf{r}}{\rho} \,. \tag{88}$$

The normalized radial coordinate ρ' is then obtained as:

$$\rho' = \frac{\rho}{a} = \frac{1}{a}\left|(\mathbf{r} - \mathbf{x}_i) - z\,\hat{\mathbf{e}}_z\right| \,. \tag{89}$$

16

The magnetic field of the straight wire segment consists of the tangential component B_φ:

$$\mathbf{B}(\mathbf{r}) = B_\varphi \hat{\mathbf{e}}_\varphi \tag{90}$$

with $\hat{\mathbf{e}}_\varphi = \hat{\mathbf{e}}_z \times \hat{\mathbf{e}}_\rho$. The magnetic vector potential only has a component in parallel direction in the coordinate system of the wire segment. The vector potential of the circular wire loop in thus in Cartesian coordinates:

$$\mathbf{A}(\mathbf{r}) = A_z \hat{\mathbf{e}}_z \,. \tag{91}$$

2.3.2. Circular Wire Loop

Figure 4 illustrates the setup of a circular wire loop.
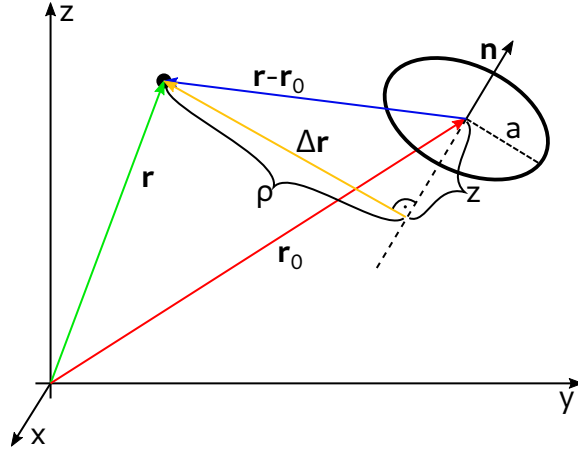
Figure 4: Mapping the components to Cartesian coordinates for an exemplary circular wire loop. The loop is centered around its origin $\mathbf{r}_0$. Its normal vector is denoted $\mathbf{n}$ and defines the orientation of the loop. The radius of the loop is denoted by a. The evaluation location is denoted by $\mathbf{r}$.

The z-axis of the wire loop's coordinate system is defined by the normal vector $\mathbf{n}$:

$$\hat{\mathbf{e}}_z = \frac{\mathbf{n}}{|\mathbf{n}|} \,. \tag{92}$$

The z component of the evaluation location is thus obtained as follows:

$$z = (\mathbf{r} - \mathbf{r}_0) \cdot \hat{\mathbf{e}}_z \,. \tag{93}$$

The normalized z-coordinate z' is then obtained as:

$$z' = \frac{z}{a} = \frac{1}{a}(\mathbf{r} - \mathbf{r}_0) \cdot \hat{\mathbf{e}}_z \,. \tag{94}$$

17

For the radial coordinate, first the vector $\Delta\mathbf{r}$ is formed:

$$\Delta\mathbf{r} = (\mathbf{r} - \mathbf{r}_0) - z\,\hat{\mathbf{e}}_z \tag{95}$$

and the radial coordinate ρ is then obtained by taking $\rho = |\Delta\mathbf{r}|$. A unit vector in radial direction is formed as follows:

$$\hat{\mathbf{e}}_\rho = \frac{\Delta\mathbf{r}}{\rho}\,. \tag{96}$$

The normalized radial coordinate ρ' is then obtained as:

$$\rho' = \frac{\rho}{a} = \frac{1}{a}|(\mathbf{r} - \mathbf{r}_0) - z\,\hat{\mathbf{e}}_z|\,. \tag{97}$$

The magnetic field of the circular wire loop consists of two cylindrical components, namely B_ρ and B_z. The Cartesian magnetic field components are then computed as follows:

$$\mathbf{B}(\mathbf{r}) = B_\rho\hat{\mathbf{e}}_\rho + B_z\hat{\mathbf{e}}_z\,. \tag{98}$$

The magnetic vector potential only has a component in angular direction in the coordinate system of the wire loop. The corresponding unit vector $\hat{\mathbf{e}}_\varphi$ is then given by $\hat{\mathbf{e}}_\varphi = \hat{\mathbf{e}}_z \times \hat{\mathbf{e}}_\rho$. The vector potential of the circular wire loop in thus in Cartesian coordinates:

$$\mathbf{A}(\mathbf{r}) = A_\varphi\hat{\mathbf{e}}_\varphi\,. \tag{99}$$

2.4. Superposition in multi-filament assemblies

An infinitely thin polygon filament P is described by a list of N points $\mathbf{x}_i$ with $i = 1, ..., N$ in three-dimensional (3D) space and a current I. The $(N-1)$ straight connecting lines between each two consecutive points $\mathbf{x}_i$ and $\mathbf{x}_{i+1}$ are assumed to represent the geometry of a wire which carries the current. If the first and the last point of the polygon filament coincide, the wire forms a closed loop and $\nabla \cdot \mathbf{j} = 0$ is ensured by construction.

The magnetic vector potential $\mathbf{A}(I, \mathbf{x}_i, \mathbf{x}_{i+1}, \mathbf{x})$ and the magnetic field $\mathbf{B}(I, \mathbf{x}_i, \mathbf{x}_{i+1}, \mathbf{x})$ of the wire segments at a location $\mathbf{x}$ can be computed analytically. The resulting contributions from each segment are superposed in order to compute the resulting magnetic field from the full length of the wire:

$$\mathbf{A}(\mathbf{x}) = \sum_{i=1}^{N-1} \mathbf{A}(I, \mathbf{x}_i, \mathbf{x}_{i+1}, \mathbf{x}) \quad \text{and} \tag{100}$$

$$\mathbf{B}(\mathbf{x}) = \sum_{i=1}^{N-1} \mathbf{B}(I, \mathbf{x}_i, \mathbf{x}_{i+1}, \mathbf{x}) \quad . \tag{101}$$

Computationally robust and efficient expressions for $\mathbf{A}(I, \mathbf{x}_i, \mathbf{x}_{i+1}, \mathbf{x})$ and $\mathbf{B}(I, \mathbf{x}_i, \mathbf{x}_{i+1}, \mathbf{x})$ are given in Ref. [1]. The detailed derivation of these expressions is given below.

2.5. Verification Method

The asymptotic behavior of an implementation of above formulas for the magnetic vector potential and magnetic field needs to be tested before using that implementation in daily routine work.

A set of critical test points used to check this is shown in Fig. 5 for the case of the circular wire loop.
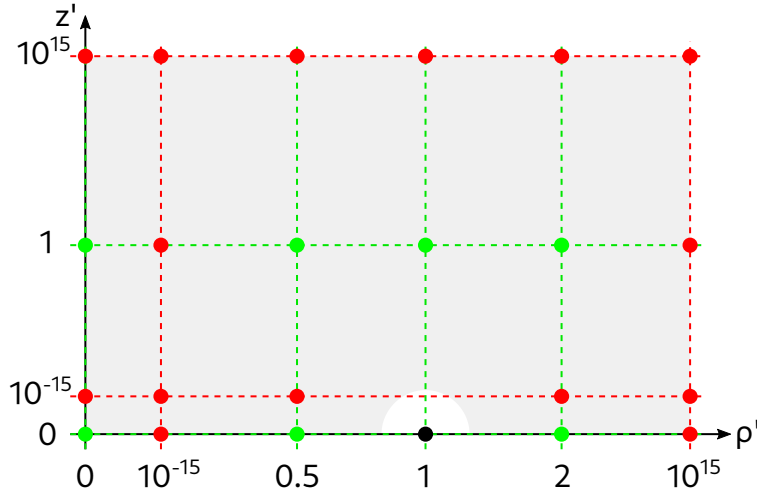
Figure 5: Test points in the R-Z-plane for a circular wire loop (black dot). The axes are labeled in normalized cylindrical coordinates ($\rho' = \rho/a$, $z' = z/a$; a is the radius of the wire loop). Green dashed lines indicate values of ρ' and z' which are well handled by a naive implementation. Green dots denote points at which a naive implementation yields satisfactory results. Red dashed lines indicate values of ρ' and z' which induce the requirement for robust asymptotic behavior. Red dots denote points at which a naive implementation usually fails. The grey shaded area in the background indicates the region in which the reference implementation yields accurate results. Note that the problem is symmetric in z direction, even though only the positive-z quadrant is considered here.

The reference results are computed on each test point using arbitrary-precision arithmetic as provided by the Python package `mpmath` [4] and Mathematica [5]. The test point coordinates are computed within the finite-precision test programs used to check the accuracy of the results. This implies

19

that the exact *implied* values of the test point coordinates have to be transported into the arbitrary-precision software used to compute the reference data. The evaluation positions are specified at IEEE754 `float64` floating-point numbers. The floating point numbers are re-constructed within the arbitrary-precision software in order to properly transport their intended value. In case of `float64`, this is done as follows for a floating-point number f:

$$f = \begin{cases} 0 & E = 0 \text{ and } M = 0 \\ (-1)^s \, 2^{E-1023} \left(1 + \frac{M}{2^{52}}\right) & \text{else} \end{cases} \tag{102}$$

where s is the sign bit, E is the exponent specified as an 11-bit unsigned integer and M is the mantissa specified as a 52-bit unsigned integer. Several special cases are defined for certain values of s, E and M, but in the context of this work only the case $E = 0$, $M = 0$ (s arbitrary), which represents an exact zero, is relevant. The organization of those bits in a `float64` number is shown in Fig. 6. In particular, a test point coordinate value f is passed to
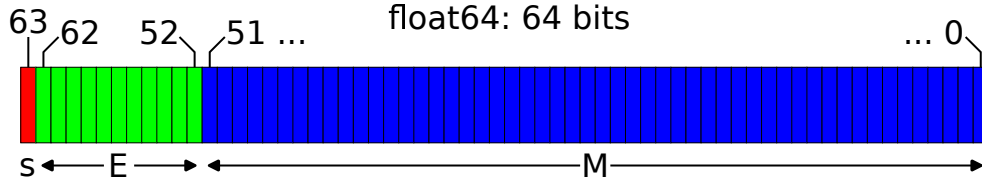

Figure 6: Organization of sign bit s, exponent E (11 bits, unsigned integer) and mantissa M (52 bits, unsigned integer) within the 64 bits of a IEEE754 `float64` floating-point number. Each box represents one bit and the colors indicate which quantity a bit belongs to (red: sign bit, green: exponent, blue: mantiassa).

the reference computation by passing the three values s, E and M as integers (which are easy to represent exactly). Within the reference computation, the value of f is constructed using Eqn. (102) implemented in arbitrary precision and with the exact values of s, E and M.

The reference data for the straight wire segment methods is computed using 300 decimal digits of precision. The reference data for the circular wire loop is computed using 200 decimal digits of precision.

The evaluation position is specified exactly via s_ρ, E_ρ and M_ρ (for ρ') and

s_z, E_z and M_z (for z'):

$$\rho' \leftarrow (-1)^{s_\rho} \, 2^{E_\rho - 1023} \left(1 + \frac{M_\rho}{2^{52}}\right)$$

$$z' \leftarrow (-1)^{s_z} \, 2^{E_z - 1023} \left(1 + \frac{M_z}{2^{52}}\right) \qquad (103)$$

The following algorithm is used to compute reference values of $\tilde{A}_z$ and $\tilde{B}_\varphi$ at (ρ', z') for the straight wire segment:

$$
\begin{aligned}
r_\mathrm{i} &\leftarrow \sqrt{\rho'^2 + z'^2} \\
r_\mathrm{f} &\leftarrow \sqrt{\rho'^2 + (1 - z')^2} \\
\epsilon &\leftarrow (r_\mathrm{i} + r_\mathrm{f})^{-1} \\
\tilde{A}_z &\leftarrow \operatorname{atanh}(\epsilon) \\
\tilde{B}_\varphi &\leftarrow \left(\frac{1}{r_\mathrm{i}} + \frac{1}{r_\mathrm{f}}\right) \frac{\rho'}{r_\mathrm{i} r_\mathrm{f} + \rho'^2 + z'(z' - 1)}
\end{aligned}
\qquad (104)
$$

The following algorithm is used to compute reference values of $\tilde{A}_\varphi$ and $\tilde{B}_\rho$ at (ρ', z') for the circular wire loop:

$$k_c^2 \leftarrow \frac{z'^2 + (1 - \rho')^2}{z'^2 + (1 + \rho')^2}$$

if $\rho' = 0 : \tilde{A}_\varphi = 0$; else:

$$\tilde{A}_\varphi \leftarrow \frac{1}{\sqrt{z'^2 + (1 + \rho')^2}} \int_0^{\pi/2} \frac{\sin^2(\varphi) - \cos^2(\varphi)}{\sqrt{\cos^2(\varphi) + k_c^2 \sin^2(\varphi)}} \, \mathrm{d}\varphi \qquad (105)$$

if $\rho' = 0$ or $z' = 0 : \tilde{B}_\rho = 0$; else:

$$\tilde{B}_\rho \leftarrow \frac{z'}{\left[z'^2 + (1 + \rho')^2\right]^{3/2}} \int_0^{\pi/2} \frac{\sin^2(\varphi) - \cos^2(\varphi)}{\left[\cos^2(\varphi) + k_c^2 \sin^2(\varphi)\right]^{3/2}} \, \mathrm{d}\varphi \qquad (106)$$

21

The method used to compute $\tilde{B}_z$ works slightly differently:

$$k^2 \leftarrow \begin{cases} 4/\left(\frac{1}{\rho'} + 2 + \rho'\right) & z' = 0 \\ \frac{4\rho'}{z'^2 + (1+\rho')^2} & \text{else} \end{cases}$$

$$\tilde{B}_z \leftarrow \frac{1}{\left[z'^2 + (1+\rho')^2\right]^{3/2}} \int_0^{\pi/2} \frac{(1-\rho')\sin^2(\varphi) + (1+\rho')\cos^2(\varphi)}{\left[1 - k^2 \sin^2(\varphi)\right]^{3/2}}\, \mathrm{d}\varphi \quad (107)$$

The integrals are carried out numerically within the arbitrary-precision software. In case of `mpmath`, double-exponential quadrature [6] is used [7].

The error metric employed in this work is given as follows:

$$\delta(a, b) = \begin{cases} \log_{10}\left(\min\left(1, \left|\frac{a-b}{b}\right|\right)\right) & b \neq 0, a \neq b \\ 0 & b = 0, a \neq 0 \\ -16 & \text{else} \end{cases} \quad (108)$$

22

3. Results

3.1. Further tests

A second-order correction to the polygon approximation for a circular wire loop [8] was tested. Second-order iterative Kahan-Babuska summation [9] had to be used to achive convergence down to numerical accuracy.
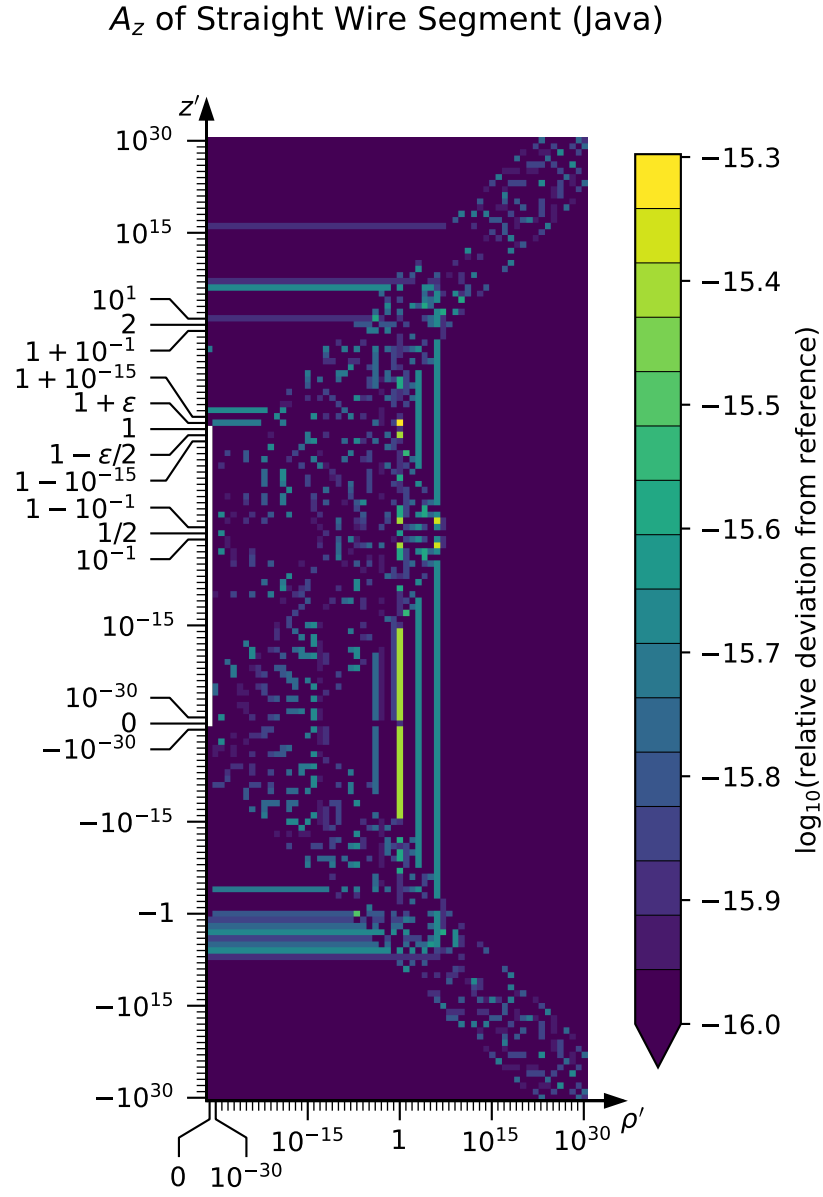
Figure 7: $\tilde{A}_z$ of straight wire segment: Comparison of the Java implementation against the reference data.
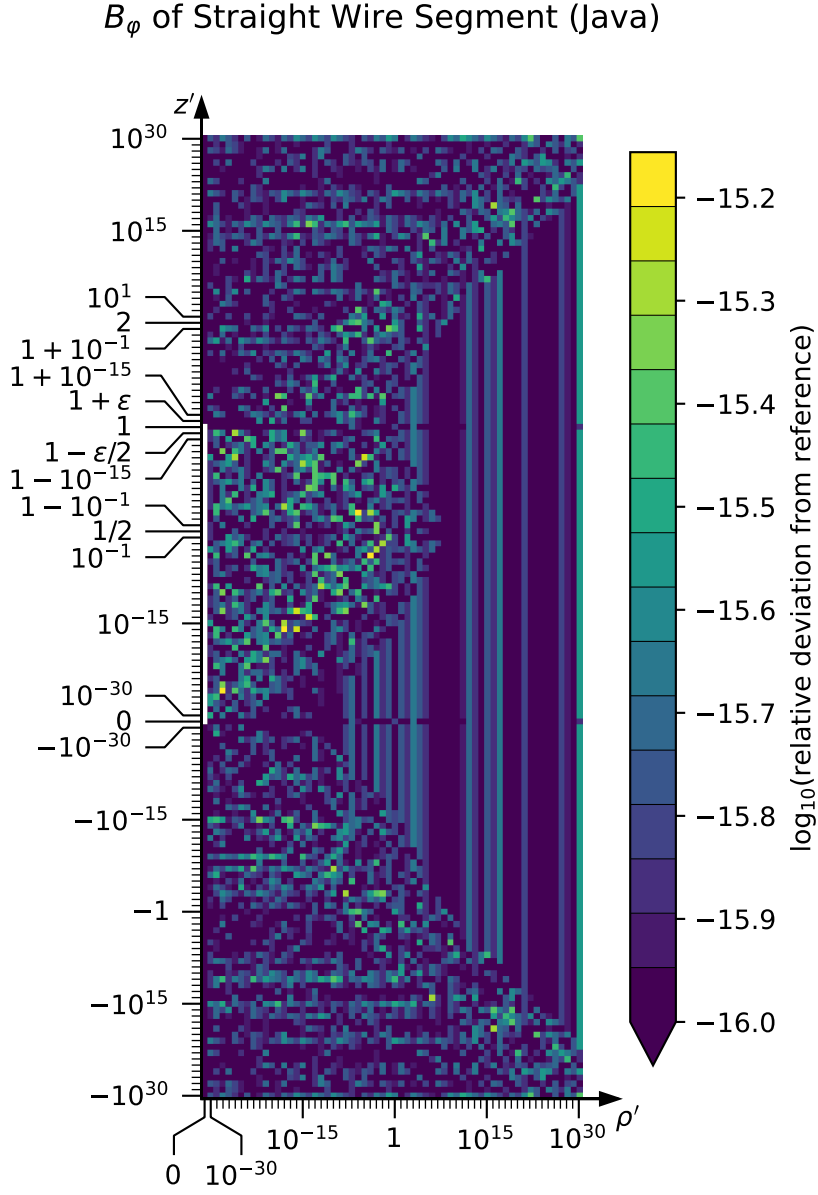
Figure 8: $\tilde{B}_\varphi$ of straight wire segment: Comparison of the Java implementation against the reference data.
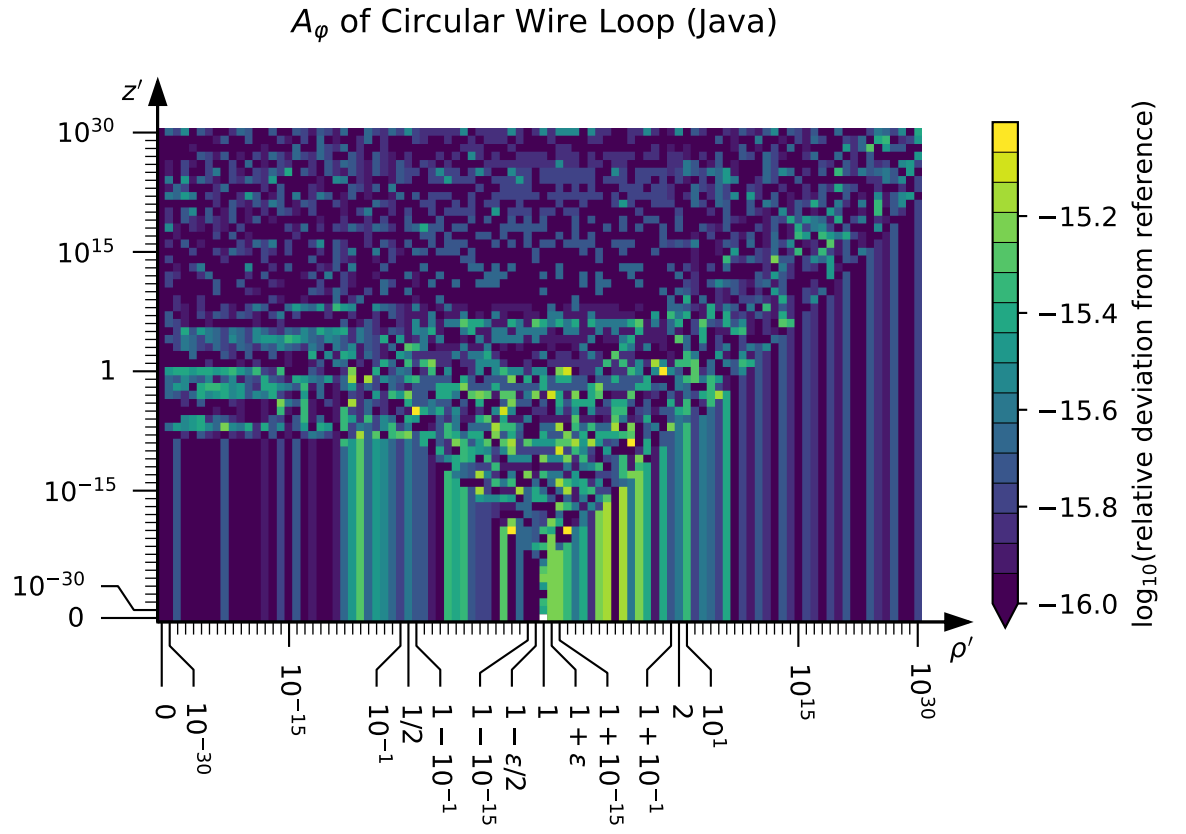
Figure 9: $\tilde{A}_{\varphi}$ of circular wire loop: Comparison of the Java implementation against the reference data.
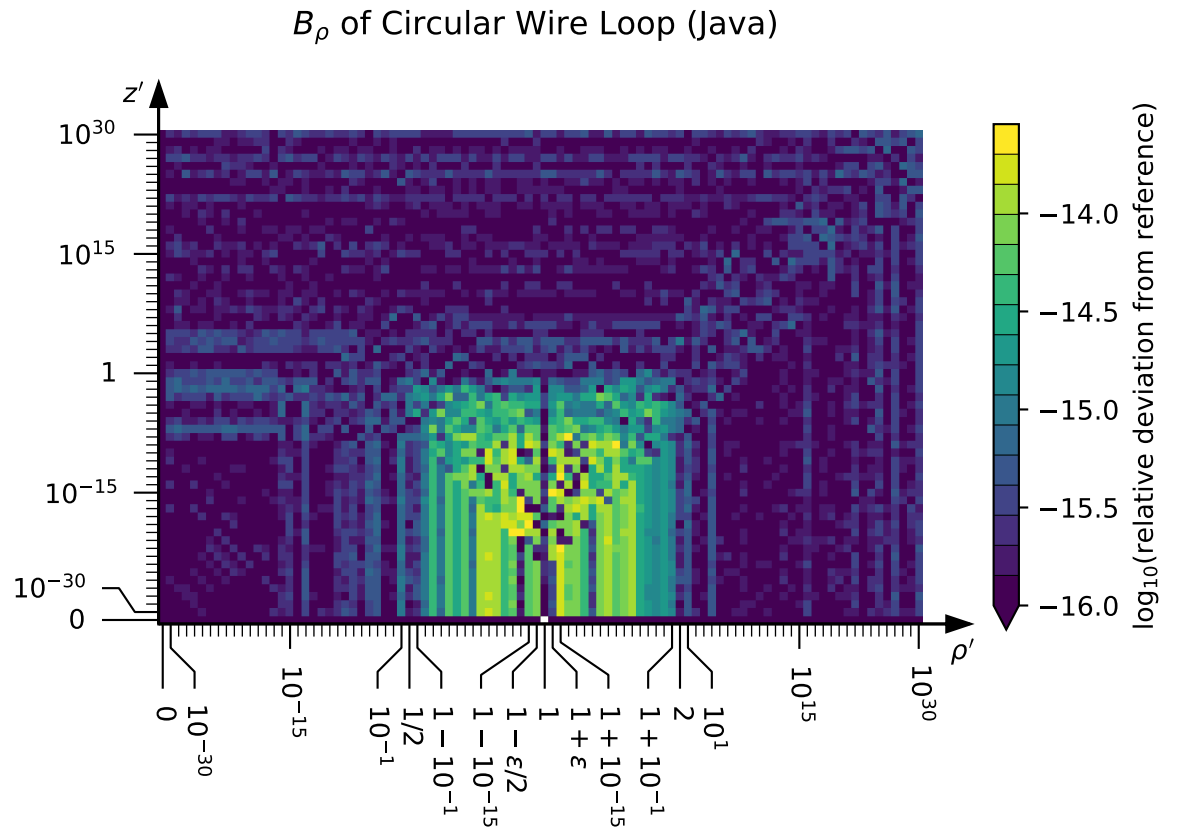
Figure 10: $\tilde{B}_\rho$ of circular wire loop: Comparison of the Java implementation against the reference data.
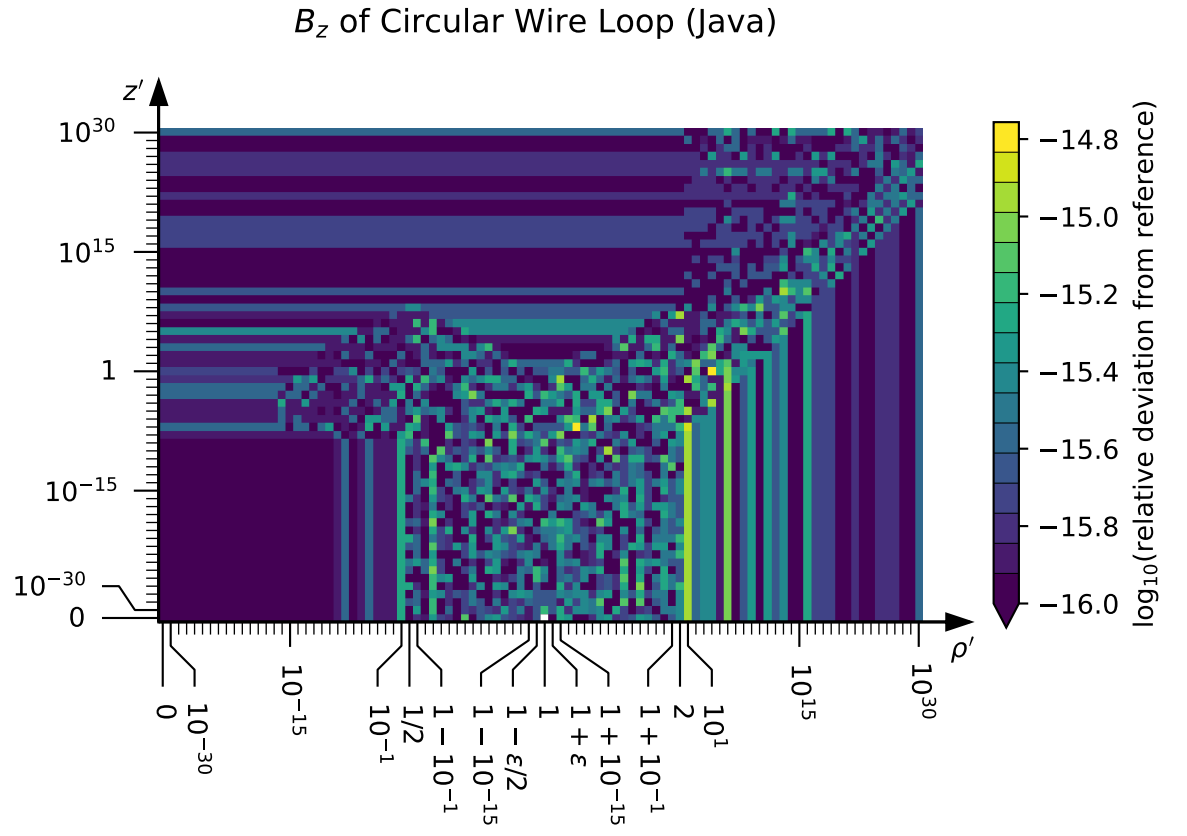
Figure 11: $\tilde{B}_z$ of circular wire loop: Comparison of the Java implementation against the reference data.

4. Discussion

It turns out that most of these problems have been considered in Ref. [10] already.

5. Concluding Remarks

Appendix A. Derivation of General Formulations

The derivations of the starting point formulas presented in Sec. 2 are given here.

Appendix A.1. Straight Wire Segment

The following geometric quantities with $\mathbf{x}_f \equiv \mathbf{x}_{i+1}$ are defined to ease the rest of the derivation:

$$L \equiv |\mathbf{x}_f - \mathbf{x}_i|, \tag{A.1}$$

$$\hat{\mathbf{e}} \equiv (\mathbf{x}_f - \mathbf{x}_i)/L, \tag{A.2}$$

$$\mathbf{R}_i \equiv \mathbf{x} - \mathbf{x}_i, \tag{A.3}$$

$$\mathbf{R}_f \equiv \mathbf{x} - \mathbf{x}_f, \tag{A.4}$$

$$R_i \equiv |\mathbf{R}_i| = |\mathbf{x} - \mathbf{x}_i|, \tag{A.5}$$

$$R_f \equiv |\mathbf{R}_f| = |\mathbf{x} - \mathbf{x}_f|, \tag{A.6}$$

$$R_{i||} \equiv \hat{\mathbf{e}} \cdot \mathbf{R}_i, \tag{A.7}$$

$$R_{f||} \equiv \hat{\mathbf{e}} \cdot \mathbf{R}_f, \tag{A.8}$$

$$\mathbf{R}_\perp \equiv \mathbf{R}_i - R_{i||}\hat{\mathbf{e}}, \tag{A.9}$$

$$R_\perp \equiv |\mathbf{R}_\perp| \quad \text{and} \tag{A.10}$$

$$\mathbf{c}(\lambda) \equiv \mathbf{x}_i + \lambda(\mathbf{x}_f - \mathbf{x}_i) \quad \text{for} \quad 0 \le \lambda \le 1. \tag{A.11}$$

The following relations are also needed:

$$L = R_{i||} - R_{f||} \tag{A.12}$$

$$R_i^2 - R_f^2 = L\left(R_{i||} + R_{f||}\right) \tag{A.13}$$

$$\Rightarrow R_{i||} = \frac{R_i^2 - R_f^2}{2L} + \frac{L}{2} \tag{A.14}$$

$$\Rightarrow R_{f||} = \frac{R_i^2 - R_f^2}{2L} - \frac{L}{2} \tag{A.15}$$

Appendix A.1.1. Magnetic Vector Potential

The law of Biot and Savart for the magnetic vector potential of a current density distribution $\mathbf{j}(\mathbf{x})$ is as follows [2]:

$$\mathbf{A}(\mathbf{x}) = \frac{\mu_0}{4\pi} \int \frac{\mathbf{j}(\mathbf{x}')}{|\mathbf{x} - \mathbf{x}'|} d\mathbf{x}'. \tag{A.16}$$

The parametrization of points on the line segment $\mathbf{c}(\lambda)$ can be used to apply this to the given geometry of a wire segment:

$$\mathbf{A}(\mathbf{x}) = \frac{\mu_0 I}{4\pi} L\hat{\mathbf{e}} \int_0^1 \frac{\mathrm{d}\lambda}{|\mathbf{x} - \mathbf{c}(\lambda)|} \tag{A.17}$$

$$= \frac{\mu_0 I}{4\pi} L\hat{\mathbf{e}} \int_0^1 \frac{\mathrm{d}\lambda}{|\mathbf{x} - \mathbf{x}_i - \lambda L\hat{\mathbf{e}}|} . \tag{A.18}$$

A little bit of geometric intuition is needed to simplify the denominator of the integral:

$$\mathbf{x} - \mathbf{x}_i - \lambda L\hat{\mathbf{e}} = \mathbf{R}_i - \lambda L\hat{\mathbf{e}} \tag{A.19}$$

$$= \mathbf{R}_i - R_{i||}\hat{\mathbf{e}} + R_{i||}\hat{\mathbf{e}} - \lambda L\hat{\mathbf{e}} \tag{A.20}$$

$$= \mathbf{R}_i - R_{i||}\hat{\mathbf{e}} + \left(R_{i||} - \lambda L\right)\hat{\mathbf{e}} \tag{A.21}$$

$$= \mathbf{R}_\perp + \left(R_{i||} - \lambda L\right)\hat{\mathbf{e}} . \tag{A.22}$$

Note that, in particular, $\mathbf{R}_\perp \perp \hat{\mathbf{e}}$ and thus (since $|\hat{\mathbf{e}}| = 1$) due to Pythagoras:

$$|\mathbf{x} - \mathbf{x}_i - \lambda L\hat{\mathbf{e}}|^2 = R_\perp^2 + \left(R_{i||} - \lambda L\right)^2 \tag{A.23}$$

and finally with $R_\perp^2 = R_i^2 - R_{i||}^2$ (also due to Pythagoras):

$$|\mathbf{x} - \mathbf{x}_i - \lambda L\hat{\mathbf{e}}|^2 = R_i^2 - R_{i||}^2 + R_{i||}^2 - 2\lambda L R_{i||} + \lambda^2 L^2 \tag{A.24}$$

$$= R_i^2 - 2\lambda L R_{i||} + \lambda^2 L^2 . \tag{A.25}$$

It follows:

$$\mathbf{A}(\mathbf{x}) = \frac{\mu_0 I}{4\pi} L\hat{\mathbf{e}} \int_0^1 \frac{\mathrm{d}\lambda}{\sqrt{R_i^2 - 2\lambda L R_{i||} + \lambda^2 L^2}} . \tag{A.26}$$

For $X = ax^2 + bx + c$ with $a > 0$ the following relation holds [11]:

$$\int \frac{\mathrm{d}x}{\sqrt{X}} = \frac{1}{\sqrt{a}} \log\left(2\sqrt{aX} + 2ax + b\right) . \tag{A.27}$$

Here, $x = \lambda$, $a = L^2$, $b = -2LR_{i||}$ and $c = R_i^2$. The corresponding antiderivative of the integrand in Eqn. (A.26) is:

$$\int \frac{\mathrm{d}\lambda}{\sqrt{R_i^2 - 2\lambda L R_{i||} + \lambda^2 L^2}}$$

$$= \frac{1}{L} \log\left(2\sqrt{L^2\left(L^2\lambda^2 - 2LR_{i||}\lambda + R_i^2\right)} + 2L^2\lambda - 2LR_{i||}\right) . \tag{A.28}$$

The definite integral in Eqn. (A.26) is therefore solved by the following expression:

$$\int_0^1 \frac{\mathrm{d}\lambda}{\sqrt{R_i^2 - 2\lambda L R_{i||} + \lambda^2 L^2}} \tag{A.29}$$

$$= \frac{1}{L}\left[\quad \log\left(2\sqrt{L^2\left(L^2 - 2LR_{i||} + R_i^2\right)} + 2L^2 - 2LR_{i||}\right)\right.$$

$$\left. - \log\left(2\sqrt{L^2 R_i^2} - 2LR_{i||}\right)\right] \tag{A.30}$$

$$= \frac{1}{L}\log\left(\frac{2L\sqrt{L^2 - 2LR_{i||} + R_i^2} + 2L^2 - 2LR_{i||}}{2LR_i - 2LR_{i||}}\right) \tag{A.31}$$

Note that

$$L^2 = L(R_{i||} - R_{f||}) \tag{A.32}$$
$$= LR_{i||} - LR_{f||} \tag{A.33}$$
$$\Rightarrow -2LR_{i||} + L^2 = -2LR_{i||} + LR_{i||} - LR_{f||} \tag{A.34}$$
$$= -L(R_{i||} + R_{f||}) \tag{A.35}$$
$$= R_f^2 - R_i^2 \tag{A.36}$$
$$\Rightarrow R_f^2 = R_i^2 - 2LR_{i||} + L^2 \,. \tag{A.37}$$

Therefore:

$$\int_0^1 \frac{\mathrm{d}\lambda}{\sqrt{R_i^2 - 2\lambda L R_{i||} + \lambda^2 L^2}} = \frac{1}{L}\log\left(\frac{R_f - R_{f||}}{R_i - R_{i\,\mathrm{d}\varphi||}}\right) \,. \tag{A.38}$$

Inserting this into Eqn. (A.26) leads to the first intermediate result:

$$\mathbf{A}(\mathbf{x}) = \frac{\mu_0 I}{4\pi} L \frac{1}{L} \log\left(\frac{R_f - R_{f||}}{R_i - R_{i||}}\right) \hat{\mathbf{e}} = \frac{\mu_0 I}{4\pi} \log\left(\frac{R_f - R_{f||}}{R_i - R_{i||}}\right) \hat{\mathbf{e}} \,. \tag{A.39}$$

However, if the point $\mathbf{x}$ is located on the line extension of the wire segment, $R_i = R_{i||}$ and $R_f = R_{f||}$, which leads to a 0/0 division if this formula is directly evaluated. The solution is to cancel the singular term $(L + R_f - R_i)$,

which is also zero for points on the line extension of the wire segment, in the numerator and the denominator of Eqn. (A.39). A second look resolves this:

$$\frac{R_f - R_{f\|}}{R_i - R_{i\|}} = \frac{2L\left(R_f - R_{f\|}\right)}{2L\left(R_i - R_{i\|}\right)} = \frac{2LR_f - 2L\left(\frac{R_i^2 - R_f^2}{2L} - \frac{L}{2}\right)}{2LR_i - 2L\left(\frac{R_i^2 - R_f^2}{2L} + \frac{L}{2}\right)} \tag{A.40}$$

$$= \frac{2LR_f - R_i^2 + R_f^2 + L^2}{2LR_i - R_i^2 + R_f^2 - L^2} \tag{A.41}$$

$$= \frac{2LR_f - R_i^2 + R_f^2 + L^2 + LR_i - LR_i + R_iR_f - R_iR_f}{2LR_i - R_i^2 + R_f^2 - L^2 + LR_f - LR_f + R_iR_f - R_iR_f} \tag{A.42}$$

$$= \frac{\cancel{(L + R_f - R_i)}(R_f + R_i + L)}{\cancel{(L + R_f - R_i)}(R_f + R_i - L)} = \frac{R_f + R_i + L}{R_f + R_i - L}. \tag{A.43}$$

It follows for the vector potential expression:

$$\mathbf{A}(\mathbf{x}) = \frac{\mu_0 I}{4\pi} \log\left(\frac{R_f + R_i + L}{R_f + R_i - L}\right) \hat{\mathbf{e}}. \tag{A.44}$$

The authors of Ref. [1] suggest to normalize the length of the wire segment:

$$\frac{R_f + R_i + L}{R_f + R_i - L} = \frac{1 + \epsilon}{1 - \epsilon} \quad \text{with } \epsilon \equiv \frac{L}{R_i + R_f}, \tag{A.45}$$

leading to

$$\mathbf{A}(\mathbf{x}) = \frac{\mu_0 I}{4\pi} \log\left(\frac{1 + \epsilon}{1 - \epsilon}\right) \hat{\mathbf{e}}. \tag{A.46}$$

This is the result for the magnetic vector potential of a filamentary wire segment presented in Ref. [1]. Note that

$$\text{artanh}\left(\epsilon\right) = \frac{1}{2} \log\left(\frac{1 + \epsilon}{1 - \epsilon}\right), \tag{A.47}$$

leading to

$$\boxed{\mathbf{A}(\mathbf{x}) = \frac{\mu_0 I}{2\pi} \text{artanh}\left(\epsilon\right) \hat{\mathbf{e}}}. \tag{A.48}$$

Appendix A.1.2. Magnetic Field

The law of Biot and Savart for the magnetic field of a current density distribution $\mathbf{j}(\mathbf{x})$ is as follows [2]:

$$\mathbf{B}(\mathbf{x}) = \frac{\mu_0}{4\pi} \int \mathbf{j}(\mathbf{x}') \times \frac{\mathbf{x} - \mathbf{x}'}{|\mathbf{x} - \mathbf{x}'|^3} d\mathbf{x}' . \tag{A.49}$$

The magnetic field $\mathbf{B}(\mathbf{x})$ is computed from $\mathbf{B} = \nabla \times \mathbf{A}$, applied to Eqn. (A.46). Define

$$f(\epsilon) \equiv \log \left(\frac{1 + \epsilon}{1 - \epsilon} \right) \tag{A.50}$$

and it follows:

$$\frac{4\pi}{\mu_0 I} \mathbf{B} = \nabla \times (f(\epsilon)\hat{\mathbf{e}}) = \nabla f(\epsilon) \times \hat{\mathbf{e}} + f(\epsilon) \underbrace{\nabla \times \hat{\mathbf{e}}}_{=0} = f'(\epsilon)\nabla \epsilon \times \hat{\mathbf{e}}. \tag{A.51}$$

Note that

$$\nabla \epsilon = \nabla \left(\frac{L}{R_i + R_f} \right) = \frac{-L}{(R_i + R_f)^2} \left(\nabla R_i + \nabla R_f \right)$$

$$= \frac{-L}{(R_i + R_f)^2} \left(\frac{\mathbf{R}_i}{R_i} + \frac{\mathbf{R}_f}{R_f} \right) . \tag{A.52}$$

It follows:

$$\frac{4\pi}{\mu_0 I} \mathbf{B} = f'(\epsilon) \frac{-L}{(R_i + R_f)^2} \left(\frac{\mathbf{R}_i}{R_i} + \frac{\mathbf{R}_f}{R_f} \right) \times \hat{\mathbf{e}} \tag{A.53}$$

$$= f'(\epsilon) \frac{L}{(R_i + R_f)^2} \hat{\mathbf{e}} \times \left(\frac{\mathbf{R}_i}{R_i} + \frac{\mathbf{R}_f}{R_f} \right) \tag{A.54}$$

$$= f'(\epsilon) \frac{\epsilon^2}{L} \hat{\mathbf{e}} \times \left(\frac{\mathbf{R}_i}{R_i} + \frac{\mathbf{R}_f}{R_f} \right) . \tag{A.55}$$

Also:

$$\frac{\mathbf{R}_i}{R_i} + \frac{\mathbf{R}_f}{R_f} = \frac{\mathbf{R}_i}{R_i} + \frac{\mathbf{R}_i - L\hat{\mathbf{e}}}{R_f} = \frac{R_f \mathbf{R}_i + R_i(\mathbf{R}_i - L\hat{\mathbf{e}})}{R_i R_f}$$

$$= \frac{(R_f + R_i)\mathbf{R}_i + R_i L\hat{\mathbf{e}}}{R_i R_f} = \frac{R_f + R_i}{R_i R_f} \mathbf{R}_i + \frac{R_i L}{R_i R_f} \hat{\mathbf{e}} \tag{A.56}$$

35

and therefore:

$$\hat{\mathbf{e}} \times \left(\frac{\mathbf{R}_i}{R_i} + \frac{\mathbf{R}_f}{R_f} \right) = \hat{\mathbf{e}} \times \left(\frac{R_f + R_i}{R_i R_f} \mathbf{R}_i + \frac{R_i L}{R_i R_f} \hat{\mathbf{e}} \right) = \frac{R_f + R_i}{R_i R_f} \hat{\mathbf{e}} \times \mathbf{R}_i , \quad (A.57)$$

since $\hat{\mathbf{e}} \times \hat{\mathbf{e}} = 0$. Inserting this into Eqn. (A.55) leads to:

$$\frac{4\pi}{\mu_0 I} \mathbf{B} = f'(\epsilon) \frac{\epsilon^2}{L} \frac{R_f + R_i}{R_i R_f} \hat{\mathbf{e}} \times \mathbf{R}_i = f'(\epsilon) \frac{\epsilon}{R_i R_f} \hat{\mathbf{e}} \times \mathbf{R}_i \quad (A.58)$$

Next, look at $f'(\epsilon)$:

$$f'(\epsilon) = \frac{1 - \epsilon}{1 + \epsilon} \cdot \frac{1(1 - \epsilon) - (1 + \epsilon)(-1)}{(1 - \epsilon)^2} = \frac{1 - \epsilon + 1 + \epsilon}{(1 + \epsilon)(1 - \epsilon)} = \frac{2}{1 - \epsilon^2} \quad (A.59)$$

and insert this into Eqn. (A.58):

$$\frac{4\pi}{\mu_0 I} \mathbf{B} = \frac{2\epsilon}{1 - \epsilon^2} \cdot \frac{1}{R_i R_f} \hat{\mathbf{e}} \times \mathbf{R}_i \quad (A.60)$$

$$= \frac{2L}{R_i + R_f} \cdot \frac{(R_i + R_f)^2}{(R_i + R_f)^2 - L^2} \cdot \frac{1}{R_i R_f} \hat{\mathbf{e}} \times \mathbf{R}_i . \quad (A.61)$$

This results in the final expression for the magnetic field:

$$\boxed{\mathbf{B}(\mathbf{x}) = \frac{\mu_0 I}{4\pi} \frac{2L(R_i + R_f)}{R_i R_f} \frac{1}{(R_i + R_f)^2 - L^2} \hat{\mathbf{e}} \times \mathbf{R}_i .} \quad (A.62)$$

Appendix B. Derivation of Special Case Formulations

The derivation of the circular wire loop formulas is considered first. It starts at the expression given by Jackson [2] and listed here in Eqn. (41). Normalized coordinates (ρ', z') as introduced above are used to reformulate the expression given by Jackson into the following:

$$A_\varphi(\rho', z') = \frac{\mu_0 I}{\pi} \frac{1}{\sqrt{z'^2 + (1 + \rho')^2}} \left[\frac{(2 - k^2)\mathcal{K}(k) - 2\mathcal{E}(k)}{k^2} \right] . \quad (B.1)$$

According to Eqn. (52), a normalizing prefactor is split off. The remaining term $\tilde{A}_\varphi(\rho', z')$ only depends on the geometry of the wire loop and the evalation location:

$$\tilde{A}_\varphi(\rho', z') = \frac{1}{\sqrt{z'^2 + (1 + \rho')^2}} \left[\frac{(2 - k^2)\mathcal{K}(k) - 2\mathcal{E}(k)}{k^2} \right] . \quad (B.2)$$

36

Cancellations can happen in the numerical evaluation of Eqn. (B.2) [3]. Therefore, another form for $\tilde{A}_\varphi(\rho', z')$ can be found by employing formulas from Ref. [12] (Section V.B.11 on page 73 therein):

$$\mathcal{K}(k) = \mathcal{E}(k) + k^2 \mathcal{D}(k)$$

$$\Leftrightarrow \mathcal{D}(k) = \frac{\mathcal{K}(k) - \mathcal{E}(k)}{k^2} \tag{B.3}$$

$$2\mathcal{D}(k) = \mathcal{K}(k) + k^2 \mathcal{C}(k)$$

$$\Leftrightarrow k^2 \mathcal{C}(k) = 2\mathcal{D}(k) - \mathcal{K}(k)$$

$$= 2\left(\frac{\mathcal{K}(k) - \mathcal{E}(k)}{k^2}\right) - \mathcal{K}(k)$$

$$= \frac{(2 - k^2)\mathcal{K}(k) - 2\mathcal{E}(k)}{k^2}. \tag{B.4}$$

Application of Eqn. (B.4) to Eqn. (B.2) leads to:

$$\tilde{A}_\varphi(\rho', z') = \frac{k^2}{\sqrt{z'^2 + (1 + \rho')^2}}\, \mathcal{C}(k). \tag{B.5}$$

This is the far-field method used in Eqn. (55). Note that $\mathcal{C}(k)$ can be evaluated as follows [13, 3]:

$$\mathcal{C}(k) = \text{cel2}\left(\frac{2\sqrt{|k_c|}}{1 + |k_c|}, 0, \frac{2}{(1 + |k_c|)^3}\right)$$

$$= \text{cel}\left(\frac{2\sqrt{|k_c|}}{1 + |k_c|}, 1, 0, \frac{2}{(1 + |k_c|)^3}\right). \tag{B.6}$$

The absolute value around k_c is otherwise omitted in this work because $k_c \geq 0$ always holds for the formulation of k_c used in this work. Eqn. (B.1) is a linear combination of the complete elliptic integrals of the first and second kind and can be handled by the `cel` function introduced by Bulirsch [3]:

$$\lambda \mathcal{K}(k) + \mu \mathcal{E}(k) = \text{cel}\left(k_c, 1, \lambda + \mu, \lambda + \mu k_c^2\right). \tag{B.7}$$

Here, $\lambda = (2 - k^2)/k^2$ and $\mu = -2/k^2$, leading to:

$$\lambda + \mu = \frac{2 - k^2}{k^2} - \frac{2}{k^2}$$
$$= \frac{\cancel{2} - k^2 \cancel{-2}}{k^2} = -1$$
$$\lambda + \mu k_c^2 = \frac{2 - k^2}{k^2} - \frac{2(1 - k^2)}{k^2}$$
$$= \frac{\cancel{2} - k^2 \cancel{-2} + 2k^2}{k^2} = 1 \tag{B.8}$$

Thus, $\tilde{A}_\varphi(\rho', z')$ can be expressed as follows:

$$\tilde{A}_\varphi(\rho', z') = \frac{1}{\sqrt{z'^2 + (1 + \rho')^2}} \mathrm{cel}\,(k_c, 1, -1, 1)\,. \tag{B.9}$$

This is equivalent to Eqn. (3.2.1.6) in Ref. [14]. The near-field (close to $\rho' = 1$) is handled by factoring out $|\rho' - 1|$:

$$\tilde{A}_\varphi(\rho', z') = \frac{1}{|\rho' - 1|\sqrt{\left(\frac{z'}{\rho'-1}\right)^2 + \left(1 + \frac{2}{\rho'-1}\right)^2}} \mathrm{cel}\,(k_c, 1, -1, 1) \tag{B.10}$$

with

$$k_c^2 = \frac{\left(\frac{z'}{\rho'-1}\right)^2 + 1}{\left(\frac{z'}{\rho'-1}\right)^2 + \left(1 + \frac{2}{\rho'-1}\right)^2}\,, \tag{B.11}$$

where the following was used:

$$\frac{\rho' + 1}{\rho' - 1} = \frac{\rho' - 1 + 2}{\rho' - 1} = 1 + \frac{2}{\rho' - 1}\,. \tag{B.12}$$

The formulation presented in Eqn. (B.10) is used in Eqn. (57).

Appendix C. Reference Data

Reference outputs have been computed using the `mpmath` Python package [4]. The reference implementation was tested at a subset of the test points against Mathematica [5]. The results are listed in Table C.1.

case	ρ'	z'	A_φ / Tm
0	0	0	`0.0000000000000000e+00`
1	10^{-15}	0	`3.5499996985564660e-20`
2	0.5	0	`1.9733248350774467e-05`
3	2	0	`9.8666241753872340e-06`
4	10^{15}	0	`3.5499996985564664e-35`
5	0	10^{-15}	`0.0000000000000000e+00`
6	10^{-15}	10^{-15}	`3.5499996985564660e-20`
7	0.5	10^{-15}	`1.9733248350774467e-05`
8	2	10^{-15}	`9.8666241753872340e-06`
9	10^{15}	10^{-15}	`3.5499996985564664e-35`
10	0	1	`0.0000000000000000e+00`
11	10^{-15}	1	`1.2551144300297384e-20`
12	0.5	1	`5.8203906810256120e-06`
13	1	1	`8.8857583532073070e-06`
14	2	1	`6.2831799875378960e-06`
15	10^{15}	1	`3.5499996985564664e-35`
16	0	10^{15}	`0.0000000000000000e+00`
17	10^{-15}	10^{15}	`3.5499996985564664e-65`
18	0.5	10^{15}	`1.7749998492782333e-50`
19	1	10^{15}	`3.5499996985564666e-50`
20	2	10^{15}	`7.0999993971129330e-50`
21	10^{15}	10^{15}	`1.2551144300297385e-35`

Table C.1: Reference outputs for testing an implementation of Eqn. (105), computed using arbitrary-precision arithmetic. The displayed values for A_φ are rounded to the nearest 64-bit `double` precision value (IEEE 754). The loop current was chosen as $I = 113\,\mathrm{A}$.

References

[1] J. D. Hanson, S. P. Hirshman, Compact expressions for the Biot-Savart fields of a filamentary segment, Physics of Plasmas 9 (2012) 4410–4412. `doi:10.1063/1.1507589`.

[2] J. D. Jackson, Classical Electrodynamics, 5th Edition, Wiley, New York, NY, 2014.

[3] R. Bulirsch, Numerical Calculation of Elliptic Integrals and Elliptic Functions. III 13 (1969) 305 – 315. `doi:10.1007/BF02165405`.

[4] F. Johansson, et al., mpmath: a Python library for arbitrary-precision floating-point arithmetic (version 0.18), `http://mpmath.org/` (December 2013).

[5] Wolfram Research, Inc., Mathematica, Version 12.1, Champaign, IL, 2021.
URL `https://www.wolfram.com/mathematica`

[6] T. Hidetosi, M. Masatake, Double exponential formulas for numerical integration, Publ. Res. Inst. Math. Sci. 9 (1973) 721 – 741. `doi:10.2977/prims/1195192451`.

[7] F. Johansson, et al., Numerical integration (quadrature) - mpmath 1.2.0 documentation, accessed 2022-05-25.
URL `https://mpmath.org/doc/current/calculus/integration.html`

[8] N. McGreivy, C. Zhu, L. M. Gunderson, S. R. Hudson, Computation of the Biot-Savart line integral with higher-order convergence using straight segments, Physics of Plasmas 28 (2021) 082111. `doi:10.1063/5.0058014`.

[9] A. Klein, A Generalized Kahan-Babuska-Summation-Algorithm, Computing 76 (2006) 279 – 293. `doi:10.1007/s00607-005-0139-x`.

[10] P. L. Walstrom, Algorithms for Computing the Magnetic Field, Vector Potential, and Field Derivatives for Circular Current Loops in Cylindrical Coordinates (2017) LA–UR–17–27619`doi:10.2172/1377379`.

[11] I. N. Bronstein, K. A. Semendjajew, Taschenbuch der Mathematik, 19th Edition, BSB B. G. Teubner Verlagsgesellschaft, Nauka-Verlag, Leipzig, Moskau, 1979.

[12] E. Jahnke, F. Emde, Tables of Functions with Formulae and Curves, 4th Edition, Dover Publications, New York, NY, 1945.

[13] R. Bulirsch, Numerical Calculation of Elliptic Integrals and Elliptic Functions. I 7 (1965) 78 – 90.

[14] J. Belcher, S. Olbert, N. Derby, TEAL Physics and Mathematics Documentation, accessed 2021-09-02 (2008).
URL `http://web.mit.edu/viz/soft/visualizations/tealsim/downloads/TEAL_Physics_Math.pdf`